Theory of Raman scattering from orbital excitations in manganese oxides

S. Okamoto,[1] S. Ishihara,[2,*] and S. Maekawa[3]
[1]*The Institute of Physical and Chemical Research (RIKEN), Saitama 351-0198, Japan*
[2]*Department of Applied Physics, University of Tokyo, Tokyo 113-8656, Japan*
[3]*Institute for Materials Research, Tohoku University, Sendai 980-8577, Japan*
(Received 1 August 2001; revised manuscript received 6 May 2002; published 19 July 2002)

We present a theory of the Raman scattering from the orbital wave excitations in manganese oxides. Two excitation processes of the Raman scattering are proposed. The Raman scattering cross sections are formulated by using the pseudospin operator for orbital degree of freedom in a Mn ion. The Raman spectra from the orbital wave excitations are calculated and their implications in the recent experimental results reported in $LaMnO_3$ are discussed.

DOI: 10.1103/PhysRevB.66.014435 PACS number(s): 75.30.Et, 75.30.Vn, 71.10.−w, 78.20.Bh

I. INTRODUCTION

Since the discovery of the colossal magnetoresistance, much attention has been attracted to manganese oxides with perovskite structure.[1–3] A variety of anomalous phenomena including gigantic decrease of the resistivity are observed in the vicinity of the phase transition from the charge and orbital ordered state to the ferromagnetic metallic one in the oxides. One of the key factors to bring about the phenomena is the orbital degree of freedom in a Mn ion.[4] Due to the strong Hund coupling and crystalline field, two e_g orbitals are degenerate and one of the $3d_{3z^2-r^2}$ and $3d_{x^2-y^2}$ orbitals is occupied by an electron in a Mn^{3+} ion.

Extensive studies of the orbital ordering have been done. It is well known that orbital ordering associated with the Jahn-Teller (JT) type lattice distortion plays an important role to stabilize the layered antiferromagnetic (A-AF) ordering in $LaMnO_3$, where spins align parallel (antiparallel) in the xy plane (along the z axis). [5–17] It has been reported that the observed orbital ordering is cooperatively stabilized by the superexchange (SE)-type electronic interaction, JT, higher-order JT and electron-strain couplings.[17] A variety of magnetic structures with the orbital orderings are also observed in the doped manganites. On the other hand, the dynamics of orbital still remains to be clarified. In the orbital ordered state, the collective electron excitations from occupied orbital to unoccupied one have been theoretically predicted.[12,18–23] This excitation is termed orbital wave (OW) and its quantized particle is called orbiton. The OW is expected to affect various low-energy properties, such as magnon[22] and phonon[23] dispersions, and transport[24]. However, the OW excitations have not been observed because the experimental technique was limited. To clarify the dynamics of the orbital degree of freedom and its effects on the physical properties in manganese oxides, it is indispensable to establish a method to observe the OW.

As a probe to observe the OW, Ishihara *et al.* proposed the resonant inelastic x-ray scattering by which dispersion relation of the OW can be detected.[25] One of the other possible methods to detect the orbital excitations is the Raman scattering.[26] Although only the excitations with the total momentum $\vec{k}_{tot}=0$ are detected, the Raman scattering has the following advantages: its energy resolution is of the order of 1 cm^{-1} which is higher than that of the resonant x-ray scattering (order of 1000 cm^{-1}) and[27] and the different modes of the excitations are distinguished by the polarization analyses of the incident and scattered photons. Recently, the Raman scattering experiment in the single crystal of $LaMnO_3$ was carried out and peak structures were found around 150 meV.[28] These spectra can be attributed to neither the multiphonon nor the magnon excitations by the detailed analyses of the polarization dependence and temperature dependence of the Raman-shift energy. Thus, a theory of the Raman scattering from the remaining degree of freedom, i.e., the orbital excitation, is required to be developed.

In this paper, we present a detailed theoretical framework of the Raman scattering from the OW excitations in orbital ordered manganites. We propose two excitation processes. One of them is analogous to that in the two-magnon Raman scattering in antiferromagnets. In contrast to the magnon Raman scattering, the intensities of the Raman spectra from one- and two-orbiton excitations are of the same order of magnitudes in this process. In another scattering process, photon induces transfer of electrons between Mn e_g and O $2p$ orbitals, and one-orbiton excitation is brought about. We formulate the scattering cross sections by using the pseudospin operator for the orbital degree of freedom in a Mn ion and calculate the Raman spectra from the OW excitations. It is shown that the recent Raman scattering experiments in $LaMnO_3$ are well explained by the OW excitations.

In Sec. II, the model Hamiltonian is introduced and dispersion relation of the OW is investigated. In Sec. III and Sec. IV, the excitation processes for the Raman scattering are proposed and the cross sections are formulated, respectively. Numerical results are presented in Sec. V, where comparison between theory and experiment is shown. The last section is devoted to the summary and discussion.

II. ORBITAL WAVE

Let us set up the model Hamiltonian describing the electronic state of manganese oxides. We consider the tight-binding Hamiltonian in the cubic lattice consisting of Mn ions. At each site, two e_g orbitals are introduced and t_{2g} electrons are treated as a localized spin ($\vec{S}_{t_{2g}}$) with $S_{t_{2g}}$

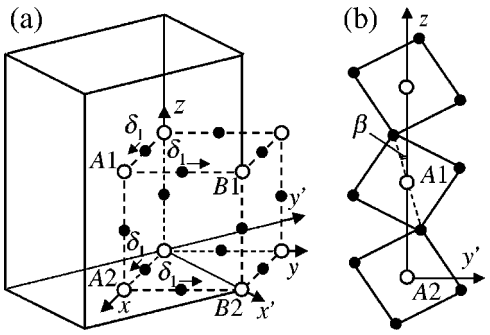

FIG. 1. (a) A unit cell of the orthorhombic structure (straight lines). Open and filled circles represent Mn and O ions, respectively. Broken lines show a unit cell of the cubic perovskite structure. Arrows indicate the displacements of O ions in the orthorhombic structures where δ_1 is an amplitude of the displacement. (b) Alternate rotations of MnO_6 octahedra around x' axis. β is an angle of the rotation.

$=3/2$. We introduce three kinds of intrasite Coulomb interactions for e_g electrons, i.e., the intra-(U) and inter-(U') orbital Coulomb interactions and the exchange interaction (I), and the energy splitting between two e_g orbitals due to the distortion of a MnO_6 octahedron. We also introduce the Hund coupling (J_H) between e_g and t_{2g} spins and the antiferromagnetic SE interaction (J_{AF}) between nearest-neighboring (NN) t_{2g} spins. Among these energy parameters, the intrasite Coulomb interactions are the largest.[29] Thus, by excluding the doubly occupied states in the e_g orbitals, the following effective Hamiltonian for the low-energy electronic state is derived:[12]

$$\tilde{\mathcal{H}}=\mathcal{H}_J+\mathcal{H}_H+\mathcal{H}_{AF}+\mathcal{H}_{JT}. \tag{1}$$

The first term represents the SE interactions between NN e_g electrons given by

$$\mathcal{H}_J=-2J_1\sum_{\langle ij\rangle}\left(\frac{3}{4}+\vec{S}_i\cdot\vec{S}_j\right)\left(\frac{1}{4}-\tau_i^l\tau_j^l\right)$$
$$-2J_2\sum_{\langle ij\rangle}\left(\frac{1}{4}-\vec{S}_i\cdot\vec{S}_j\right)\left(\frac{3}{4}+\tau_i^l\tau_j^l+\tau_i^l+\tau_j^l\right), \tag{2}$$

where J_1 and J_2 indicate the SE interactions.[30] $\vec{S}_i$ is the spin operator of the e_g electron with $S=1/2$. $\tau_i^l=\cos[(2\pi/3)m_l]T_{iz}-\sin[(2\pi/3)m_l]T_{ix}$ with $(m_x,m_y,m_z)=(1,-1,0)$. l denotes a direction of a bond connecting i and j sites. $\vec{T}_i$ is the pseudospin operator for the orbital degree of freedom.[31] $\langle T_{iz}\rangle=+(-)1/2$ corresponds to the state where the $d_{3z^2-r^2}$ ($d_{x^2-y^2}$) orbital is occupied by an electron. The second and third terms in Eq. (1) are given by

$$\mathcal{H}_H+\mathcal{H}_{AF}=-J_H\sum_i \vec{S}_i\cdot\vec{S}_{t_{2g}i}+J_{AF}\sum_{\langle ij\rangle}\vec{S}_{t_{2g}i}\cdot\vec{S}_{t_{2g}j}. \tag{3}$$

Here, the anisotropy of the SE interactions originating from the tetragonal (D_{4h}) lattice distortion is taken into account as

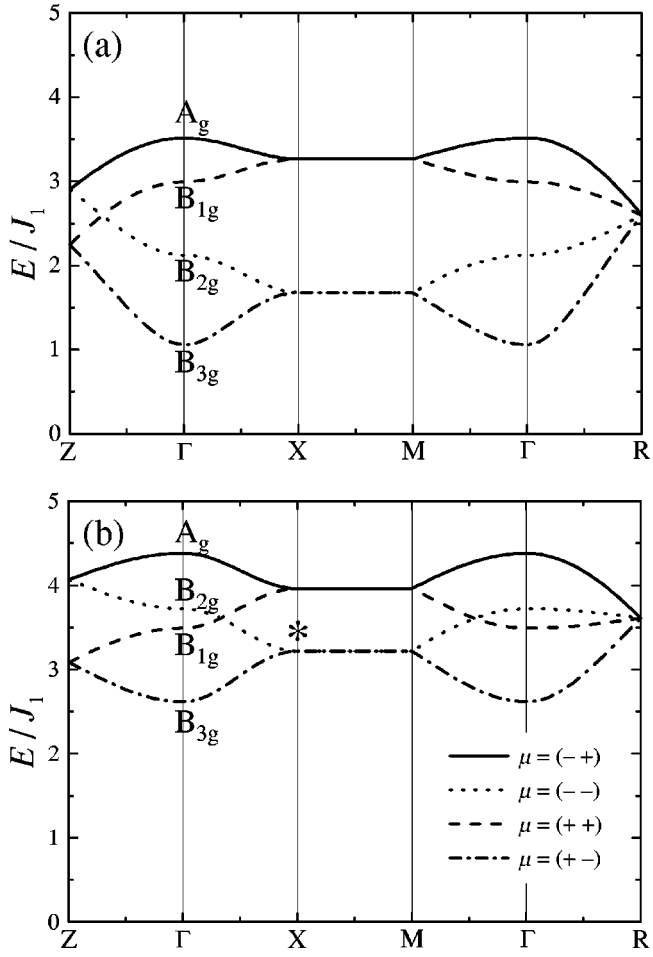

FIG. 2. Dispersion relations of OW in (a) paramagnetic and (b) A-AF phases. The Brillouin zone for the tetragonal lattice is adopted. Parameter values are chosen to be $J_2/J_1=0.35$, $R=1.07$, $g_{JT}Q/J_1=0.7$, and $\theta_{A1}^{JT}=2\pi/3$. Orbital state for the paramagnetic (A-AF) phase is denoted by $(\theta_{A1(2)},\theta_{B1(2)})=(\theta_A,-\theta_A)$ with $\theta_A=0.52\pi(0.47\pi)$. An asterisk in (b) shows the mode which becomes Raman active when the monoclinic lattice distortion is introduced (see Fig. 7).

$\sqrt{J_{1(2)}^z/J_{1(2)}^{x,y}}=\sqrt{J_{AF}^z/J_{AF}^{x,y}}=t_0^z/t_0^{x,y}=R$. t_0^ρ is the transfer intensity between NN $d_{3\rho^2-r^2}$ orbitals along the ρ axis. The last term in Eq. (1) is given by

$$\mathcal{H}_{JT}=-g_{JT}\sum_{il=z,x}Q_{il}T_{il}, \tag{4}$$

with g_{JT} being the electron-lattice coupling constant. The normal modes of the lattice distortion in a O_6 octahedron are expressed as $(Q_{iz},Q_{ix})=Q(\cos\theta_i^{JT},\sin\theta_i^{JT})$. The lattice degree of freedom is assumed to be frozen in this paper, since the electronic process that we are interested in here has much higher energy than the phonon energy which is, at most, 75 meV in $LaMnO_3$.[32,33]

We investigate the orbital states at the paramagnetic and A-AF phases by applying the mean-field approximation.[34] A unit cell with four Mn sites termed A_1, A_2, B_1, and B_2 are adopted (see Fig. 1). $A(B)$ and 1(2) classify the orbital and spin sublattices, respectively. The following spin order pa-

rameters are introduced: $\langle S_{iz}\rangle$ and $\langle S_{t_{2g}iz}\rangle (=3\langle S_{iz}\rangle)$ with $\langle\cdots\rangle$ representing the thermal average. For the JT distortion of MnO_6 octahedra, *C*-type ordering with $(\theta^{JT}_{A1(2)},\theta^{JT}_{B1(2)}) = (2\pi/3,-2\pi/3)$ is adopted by considering the observed lattice distortion in $LaMnO_3$. Even in the paramagnetic phase, due to the introduced JT coupling, the *C*-type orbital order realizes.[17] For the orbital degree of freedom, we introduce the rotating frame and adopt the order parameter as $\langle\tilde{T}_{iz}\rangle = \cos\theta^t_i\langle T_{iz}\rangle + \sin\theta^t_i\langle T_{ix}\rangle$. θ^t_i describes the orbital state at site i as $|\theta^t_i\rangle = \cos(\theta^t_i/2)|3z^2-r^2\rangle + \sin(\theta^t_i/2)|x^2-y^2\rangle$. By minimizing the energy with respect to $\{\theta^t_i\}$, we obtain $(\theta^t_{A1(2)},\theta^t_{B1(2)}) = (\theta_A,-\theta_A)$ in both the paramagnetic and *A*-AF phases.

The collective orbital excitations in the orbital ordered state are studied by applying the Holstein-Primakoff transformation to the pseudospin operators: $\tilde{T}_{iz} = 1/2 - a^\dagger_i a_i$ and $\tilde{T}_{ix} = 1/2(a^\dagger_i + a_i)$ with a_i being the bosonic operator. Here, spins are assumed to be frozen. In Figs. 2(a) and 2(b), the dispersion relations of the OW in the paramagnetic and *A*-AF states, respectively, are shown. Parameter values are chosen to be $J_2/J_1 = 0.35$, $R = 1.07$, and $g_{JT}Q/J_1 = 0.7$. J_1 is estimated to be about 50 meV from the dispersion relation of the spin wave, the Néel temperature for *A*-AF and the orbital ordering temperature.[17] It is shown that the orbital excitation has a gap in both cases. However, we note the origins of these gaps are different as follows: The gaps in paramagnetic and *A*-AF phases are given by $\{(\sqrt{3}/2)g_{JT}Q[(9/2)J_1 - (1/2)J_2 + (\sqrt{3}/2)g_{JT}Q]\}^{1/2}$ and $\{[3J_1 + (\sqrt{3}/2)g_{JT}Q)(J_1 + J_2 + (\sqrt{3}/2)g_{JT}Q]\}^{1/2}$, respectively, where θ_A is chosen to be $\pi/2$. While the gap in the paramagnetic phase decreases with decreasing $g_{JT}Q$, the gap in the *A*-AF phase remains finite. This is because the latter originates from the anisotropic magnetic structure.[12] $\mu = (a,b)$ with $a = \pm$ and $b = \pm$ in Fig. 2 denotes the mode of the OW, where a (b) represents the relative phase of the Holstein-Primakoff bosons in the xy plane (along the z axis). Among four modes, the energy of the mode $(-+)$ is the highest and its eigenoperator includes the following linear combination of the pseudospin operators:

$$\alpha^{(-+)}_{k=0} = \sqrt{\frac{N_m}{N}}\sum_l{}' \cos\theta_A\{(\cosh\theta^{(-+)} + \sinh\theta^{(-+)}) \times (T_{A1(l)x} + T_{B1(l)x} + T_{A2(l)x} + T_{B2(l)x}) + i(\cosh\theta^{(-+)} - \sinh\theta^{(-+)})(T_{A1(l)y} - T_{B1(l)y} + T_{A2(l)y} - T_{B2(l)y})\}, \quad (5)$$

where the prime indicates summation over unit cells. $\cosh\theta^{(-+)}$ and $\sinh\theta^{(-+)}$ are the coefficients of the Bogoliubov transformation. N_m is the number of sites in the unit cell. The symmetry properties of the each mode of the OW and their selection rule in the Raman scattering are presented in the Appendix.

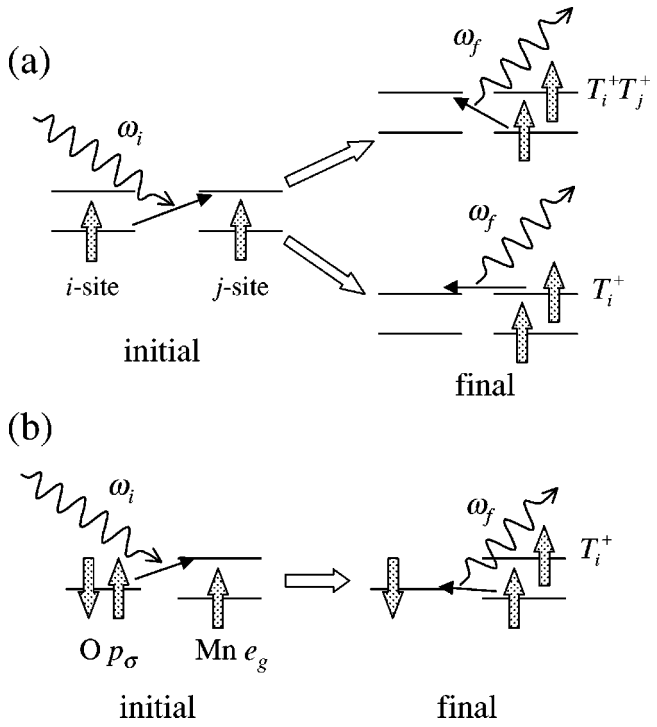

FIG. 3. (a) *d-d* and (b) *d-p* excitation processes. Wavy lines represent the incident and scattered photons with energy ω_i and ω_f, respectively. i and j in (a) represent NN Mn sites. O p_σ in (b) represents one of the six oxygen p_σ orbitals surrounding a Mn ion.

III. SCATTERING PROCESSES

It has been reported that the electronic energy bands in the region of 0–3 eV below the Fermi level in $LaMnO_3$ consist of Mn e_g and O $2p$ orbitals.[29] It is expected that both the Mn e_g and O $2p$ orbitals play important roles in the excitation processes of the Raman scattering when the visible light is used. Considering these facts, we propose the following two excitation processes.

One of the processes is analogous to that in the two-magnon Raman scattering in antiferromagnets. Mn e_g orbitals are considered and O $2p$ orbitals are integrated out. The schematic picture of this process is presented in Fig. 3(a). An electron at a Mn e_g orbital is excited to one of NN e_g orbitals through the interaction with an incident photon with energy $\hbar\omega_i$, momentum $\vec{k}_i$ and polarization λ_i. By emitting a photon with $\hbar\omega_f$, $\vec{k}_f$, and λ_f, one of the two electrons at a doubly occupied Mn site returns to the empty site. When the orbital states at one of the two or both the sites are excited, one- or two-orbiton excitations are brought about, respectively. This process is termed the *d-d* process. It is stressed that the scattering intensities from one- and two-orbiton excitations are of the same order of magnitudes due to the transfer intensity between the different orbitals. This is in contrast with the magnon Raman scattering in antiferromagnets.[35–37]

Orbital excitation is also brought about through the transfer of electrons between Mn e_g and O $2p$ orbitals. A schematic picture of this process is presented in Fig. 3(b). By absorbing an incident photon, an electron in an O p_σ orbital

is excited to the neighboring Mn e_g orbital. p_σ represents the O $2p$ orbital mixing with the Mn e_g one through the σ bond. One of the two electrons in this Mn site returns to the empty O site by emitting a photon. When the occupied orbital in the Mn site in the final state is different from that in the initial state, one-orbiton excitation is brought about. This process is termed the d-p process. In contrast to the d-d process and the magnon Raman scattering in antiferromagnets, one orbiton is excited in the d-p process.

IV. RAMAN SCATTERING CROSS SECTION

In this section, we present the formulation for the cross sections in the d-d and d-p processes.

A. d-d process

The cross section (CS) from the OW excitations is calculated in the system where the e_g electrons and photons are coupled. We adopt the following model Hamiltonian:

$$\mathcal{H}_{d-d}=\mathcal{H}_e^{d-d}+\mathcal{H}_t^{d-d}+\mathcal{H}_{ph}+\mathcal{H}_{e-ph}^{d-d}. \tag{6}$$

The first and the second terms represent the intrasite electron-electron interactions and the intersite electron transfer, respectively. These are given by

$$\mathcal{H}_e^{d-d}=\mathcal{H}_H+U\sum_{i\gamma} n_{i\gamma\uparrow}n_{i\gamma\downarrow}+U'\sum_{i\gamma\sigma\sigma'} n_{i\gamma\sigma}n_{i-\gamma\sigma'} +I\sum_{i\gamma\sigma\sigma'} d_{i\gamma\sigma}^\dagger d_{i-\gamma\sigma}^\dagger d_{i\gamma\sigma'}d_{i-\gamma\sigma}, \tag{7}$$

$$\mathcal{H}_t^{d-d}=\sum_{\substack{\langle ij\rangle\\ \gamma\gamma'\sigma}} (t_{ij}^{\gamma\gamma'}d_{i\gamma\sigma}^\dagger d_{j\gamma'\sigma}+\text{H.c.}). \tag{8}$$

$d_{i\gamma\sigma}$ is the annihilation operator of e_g electron at site i with spin σ and orbital γ. Its energy level is chosen to be zero. $t_{ij}^{\gamma\gamma'}$ is the transfer intensity between γ orbital at site i and γ' orbital at site j, and is obtained by the second-order perturbation with respect to the electron transfer between Mn e_g and O $2p$ orbitals. The explicit form of $t_{ij}^{\gamma\gamma'}$ is given by the Slater-Koster formulas.[38] The third term represents the photon system as

$$\mathcal{H}_{ph}=\sum_{\vec{k}\lambda} \hbar\omega_{\vec{k}}(b_{\vec{k}\lambda}^\dagger b_{\vec{k}\lambda}+\tfrac{1}{2}), \tag{9}$$

where $b_{\vec{k}\lambda}$ is the annihilation operator of photon with energy $\hbar\omega_{\vec{k}}$, momentum $\vec{k}$ and polarization λ. The electron-photon interaction is described by the fourth term in Eq. (6) as

$$\mathcal{H}_{e-ph}^{d-d}=-\frac{e}{c}\sum_{\langle ij\rangle\gamma\gamma'} \vec{A}\left(\frac{\vec{r}_i+\vec{r}_j}{2}\right)\cdot\vec{j}_{ij}^{\gamma\gamma'}. \tag{10}$$

Here, $\vec{A}(\vec{r})$ is the vector potential given by

$$\vec{A}(\vec{r})=\frac{1}{\sqrt{V}}\sum_{\vec{k}\lambda}\sqrt{\frac{2\pi\hbar c^2}{\omega_{\vec{k}}}}\hat{e}_\lambda(b_{\vec{k}\lambda}^\dagger e^{-i\vec{k}\vec{r}}+b_{\vec{k}\lambda}e^{i\vec{k}\vec{r}}), \tag{11}$$

with $\hat{e}_\lambda$ being the unit vector along the polarization λ. $\vec{j}_{ij}^{\gamma\gamma'}$ represents the electronic current between γ orbital at i site and γ' orbital j site given by

$$\vec{j}_{ij}^{\gamma\gamma'}=\frac{i}{\hbar}\vec{r}_{ij}t_{ij}^{\gamma\gamma'}\sum_\sigma d_{i\gamma\sigma}^\dagger d_{j\gamma'\sigma}+\text{H.c.}, \tag{12}$$

with $\vec{r}_{ij}=\vec{r}_i-\vec{r}_j$.

Being based on the Hamiltonian $\mathcal{H}_{d-d}$, the scattering matrix is calculated. The initial and final states of the scattering are described by the eigen states of $\tilde{\mathcal{H}}$ and the intermediate state is described by those of $\mathcal{H}_e^{d-d}$. The scattering matrix in the d-d process is obtained as

$$S_{fi}^{d-d}=\frac{4\pi Ci}{V}\delta(E_f-E_i)\sum_{\langle ij\rangle}\left(\hat{e}_{\lambda f}\cdot\frac{\vec{r}_{ij}}{l_{dd}}\right)\left(\hat{e}_{\lambda i}\cdot\frac{\vec{r}_{ij}}{l_{dd}}\right) \times\{2\tilde{J}_1(\tfrac{3}{4}+\vec{S}_i\cdot\vec{S}_j)(\tfrac{1}{4}-\tau_i^l\tau_j^l) +2\tilde{J}_2(\tfrac{1}{4}-\vec{S}_i\cdot\vec{S}_j)(\tfrac{3}{4}+\tau_i^l\tau_j^l+\tau_i^l+\tau_j^l)\}, \tag{13}$$

with $C=\pi e^2/(\hbar^2\sqrt{\omega_{\vec{k}_i}\omega_{\vec{k}_f}})$. $E_{i(f)}$ represents the energy of the initial (final) state. $\tilde{J}_1$ and $\tilde{J}_2$ are defined as $\tilde{J}_1=l_{dd}^2t_0^2/(U'-I+\hbar\omega_{\vec{k}_f})+l_{dd}^2t_0^2/(U'-I-\hbar\omega_{\vec{k}_i})$ and $\tilde{J}_2=l_{dd}^2t_0^2/(U+2J_H+\hbar\omega_{\vec{k}_f})+l_{dd}^2t_0^2/(U+2J_H-\hbar\omega_{\vec{k}_i})$, respectively, where l_{dd} is the distance between NN Mn sites. We rewrite the pseudospin operators in Eq. (13) by using the Holstein-Primakoff bosons, and obtain the CS. The CS from the one-orbiton excitation is given by

$$I_1^{d-d}=\frac{\omega_f^2C^2N}{\hbar(2\pi c^2)^2}\frac{4}{N_m}\sum_{\mu=1}^{N_m}\left|\sum_{\rho\nu\nu'}(\hat{e}_{\lambda f}\cdot\vec{\rho})(\hat{e}_{\lambda i}\cdot\vec{\rho})K_{\nu\nu'}^\rho\{V_{\nu\mu}(0) +W_{\nu\mu}(0)\}\right|^2\{n_{\mu0}\delta(\Delta E+\varepsilon_{\mu0}) +(1+n_{\mu0})\delta(\Delta E-\varepsilon_{\mu0})\}, \tag{14}$$

where $\vec{\rho}=\hat{x},\hat{y},\hat{z}$. $K_{\nu\nu'}^\rho$ is given by

$$K_{\nu\nu'}^\rho=\tilde{J}_1(\tfrac{3}{4}+S_\rho)S_\nu^\rho C_{\nu'}^\rho-\tilde{J}_2(\tfrac{1}{4}-S_\rho)(S_\nu^\rho C_{\nu'}^\rho+S_\nu^\rho), \tag{15}$$

with $S_\rho=\langle\vec{S}_i\cdot\vec{S}_{i+\vec{\rho}}\rangle$, $S_\nu^\rho=\sin[\theta_\nu^t+(2\pi/3)m_\rho]$, and $C_\nu^\rho=\cos[\theta_\nu^t+(2\pi/3)m_\rho]$. $V_{\nu\mu}(\vec{k})$ and $W_{\nu\mu}(\vec{k})$ are the coefficients of the Bogoliubov transformation connecting the boson operator for the νth ion to that for the μth eigenmode with the energy $\varepsilon_{\mu\vec{k}}$ as

$$a_{\nu\vec{k}}=V_{\nu\mu}(\vec{k})\alpha_{\mu\vec{k}}+W_{\nu\mu}(\vec{k})\alpha_{\mu-\vec{k}}^\dagger. \tag{16}$$

$n_{\mu\vec{k}}$ is the Bose distribution function and $\Delta E(=\hbar\omega_{\vec{k}_i}-\hbar\omega_{\vec{k}_f})$ represents the Raman-shift energy. The CS from the two-orbiton excitation is given by

$$I_2^{d-d}=\frac{\omega_f^2C^2N}{\hbar(2\pi c^2)^2}\frac{4}{N_m}\sum_{\vec{k}\mu\mu'}\Bigg|\sum_{\rho\nu\nu'}(\hat{e}_{\lambda f}\cdot\vec{\rho})(\hat{e}_{\lambda i}\cdot\vec{\rho})\times[L^{\rho}_{\nu\nu'}V_{\nu\mu}(\vec{k})W_{\nu\mu}(-\vec{k})+M^{\rho}_{\nu\nu'}(\vec{k})\delta_{\nu,\nu'+\rho}\{V_{\nu\mu}(\vec{k})+W_{\nu\mu}(\vec{k})\}\{V_{\nu'\mu'}(-\vec{k})+W_{\nu'\mu'}(-\vec{k})\}]\Bigg|^2\times(1+n_{\mu\vec{k}})(1+n_{\mu'-\vec{k}})\delta(\Delta E-\varepsilon_{\mu\vec{k}}-\varepsilon_{\mu'-\vec{k}}),\quad(17)$$

with

$$L^{\rho}_{\nu\nu'}=\tilde{J}_1(\tfrac{3}{4}+S_\rho)C^{\rho}_{\nu}C^{\rho}_{\nu'}-\tilde{J}_2(\tfrac{1}{4}-S_\rho)(C^{\rho}_{\nu}C^{\rho}_{\nu'}+2C^{\rho}_{\nu}),\quad(18)$$

$$M^{\rho}_{\nu\nu'}(\vec{k})=2\{\tilde{J}_1(\tfrac{3}{4}+S_\rho)-\tilde{J}_2(\tfrac{1}{4}-S_\rho)\}S^{\rho}_{\nu}S^{\rho}_{\nu'}\cos k_\rho.\quad(19)$$

In Eq. (17), the anti-Stokes parts are neglected for simplicity. The interaction between two orbitons in the final state is neglected. This interaction is expected to shift the two-orbiton Raman spectrum to the lower-energy region as the magnon-magnon interaction does in the two-magnon Raman scattering.[36]

B. *d-p* process

To calculate the CS, let us start with the following model Hamiltonian where Mn e_g and O p_σ orbitals and the electron-photon coupling are taken into account,

$$\mathcal{H}_{d-p}=\mathcal{H}_e^{d-p}+\mathcal{H}_t^{d-p}+\mathcal{H}_{ph}+\mathcal{H}_{e-ph}^{d-p}.\quad(20)$$

The first and second terms describe the intrasite electron-electron interactions and electron hopping as $\mathcal{H}_e^{d-p}=\mathcal{H}_e^{d-d}+\frac{1}{2}\Sigma_{i\delta\sigma}\Delta p^{\dagger}_{i\delta\sigma}p_{i\delta\sigma}$ and

$$\mathcal{H}_t^{d-p}=\sum_{i\gamma\delta\sigma}(t_{\gamma\delta}d^{\dagger}_{i\gamma\sigma}p_{i\delta\sigma}+\text{H.c.}),\quad(21)$$

respectively, where Δ is the energy level of O p_σ orbital, and $p_{i\delta\sigma}$ is the annihilation operator of the p_σ electron with σ spin at $\vec{r}_i+l_{pd}\vec{\delta}_i$. l_{pd} is the distance between NN Mn and O sites. $\vec{\delta}_i$ is the unit vector along the local $\pm x(y,z)$ direction reflecting the rotation of MnO_6. $t_{\gamma\delta}$ represents the transfer intensity between NN Mn e_g and O p_σ orbitals and is given by

$$t_{\gamma\delta}=t_{pd}\begin{pmatrix}-\frac{1}{2} & -\frac{1}{2} & 1\\ \frac{\sqrt{3}}{2} & -\frac{\sqrt{3}}{2} & 0\end{pmatrix}_{\gamma\delta},\quad(22)$$

for $\delta=x,y,z$ and $t_{\gamma\delta}=-t_{\gamma,-\delta}$. t_{pd} is the transfer intensity between Mn $d_{3z^2-r^2}$ orbital at $\vec{r}_i$ and O p_z orbital at $\vec{r}_i+l_{pd}\hat{z}_i$. The electron-photon interaction is represented by the fourth term in Eq. (20),

$$\mathcal{H}_{e-ph}^{d-p}=-\frac{e}{c}\sum_{i\gamma\delta}\vec{A}(\vec{r}_i)\cdot\vec{j}_{i\gamma\delta}.\quad(23)$$

$\vec{j}_{i\gamma\delta}$ is the current operator representing the transition between Mn γ orbital at $\vec{r}_i$ and O p_σ orbital at $\vec{r}_i+l_{pd}\vec{\delta}_i$ given by

$$\vec{j}_{i\gamma\delta}=\frac{i}{\hbar}l_{pd}\vec{\delta}_i t_{\gamma\delta}\sum_{\sigma}d^{\dagger}_{i\gamma\sigma}p_{i\delta\sigma}+\text{H.c.}\quad(24)$$

The scattering matrix is obtained by the second-order perturbation with respect to $\mathcal{H}_{e-ph}^{d-p}$ and is given by

$$S_{fi}^{d-p}=\frac{4\pi Ci}{V}\delta(E_f-E_i)\sum_{i\rho}(\hat{e}_{\lambda f}\cdot\vec{\rho}_i)(\hat{e}_{\lambda i}\cdot\vec{\rho}_i)\tilde{J}\tau_i^{\rho},\quad(25)$$

where $\vec{\rho}_i=\hat{x}_i,\hat{y}_i,\hat{z}_i$ and $\tilde{J}=\frac{1}{2}l_{pd}^2t_{pd}^2\Sigma_\Omega\{3(U'-I-3/4J_H-\Delta+\hbar\Omega)^{-1}-(U+5/4J_H-\Delta+\hbar\Omega)^{-1}\}$ with $\Omega=\omega_{\vec{k}_f},-\omega_{\vec{k}_i}$. It is worth to mention that S_{fi}^{d-p} includes the linear term of τ_i because the orbital excitation is brought about in a MnO_6 octahedron. Therefore, one-orbiton excitation contributes to the Raman scattering. Finally, we rewrite the pseudospin operators in Eq. (25) by using the Holstein-Primakoff bosons, and obtain the CS in the *d-p* process as follows:

$$I^{d-p}=\frac{\omega_f^2C^2N}{\hbar(2\pi c^2)^2}\tilde{J}^2\frac{4}{N_m}\sum_{\mu}\Bigg|\sum_{\rho\nu}(\hat{e}_{\lambda f}\cdot\vec{\rho}_\nu)\times(\hat{e}_{\lambda i}\cdot\vec{\rho}_\nu)S^{\rho}_{\nu}\{V_{\nu\mu}(0)+W_{\nu\mu}(0)\}\Bigg|^2\times\{n_{\mu0}\delta(\Delta E+\varepsilon_{\mu0})+(1+n_{\mu0})\delta(\Delta E-\varepsilon_{\mu0})\}.\quad(26)$$

V. NUMERICAL RESULTS

In this section, we present the numerical results for the Raman spectra.

A. *d-d* process

Numerical results for the Raman spectra given by the summation of I_1^{d-d} and I_2^{d-d} are presented in Fig. 4. Figures 4(a), 4(b) and 4(c), 4(d) are the results in the paramagnetic and *A*-AF phases, respectively. I_0^{d-d} is defined as $I_0^{d-d}=\omega_f^2C^2N/[\hbar(2\pi)^2]\tilde{J}_1^2$ and is assumed to be independent of ω_i and ω_f, for simplicity. Parameter value is chosen to be $\tilde{J}_2/\tilde{J}_1=0.35$. Other parameter values are the same as those in Fig. 2. Sharp spectra in the region $3.0<\Delta E/J_1<3.6$ ($3.5<\Delta E/J_1<4.5$) and broad ones in the region $2.0<\Delta E/J_1<7.0$ ($5.0<\Delta E/J_1<9.0$) in the paramagnetic (*A*-AF) phase originate from one- and two-orbiton excitations, respectively. In the (x,y) and (z,x) polarizations, the one- and two-orbiton excitations are not brought about. In these configurations, polarization of the scattered photon is perpendicular to that of the incident photon and both the polarizations are parallel to the bonds between NN Mn sites. Therefore, matrix element S_{fi}^{d-d} in Eq. (13) vanishes and orbital excitations

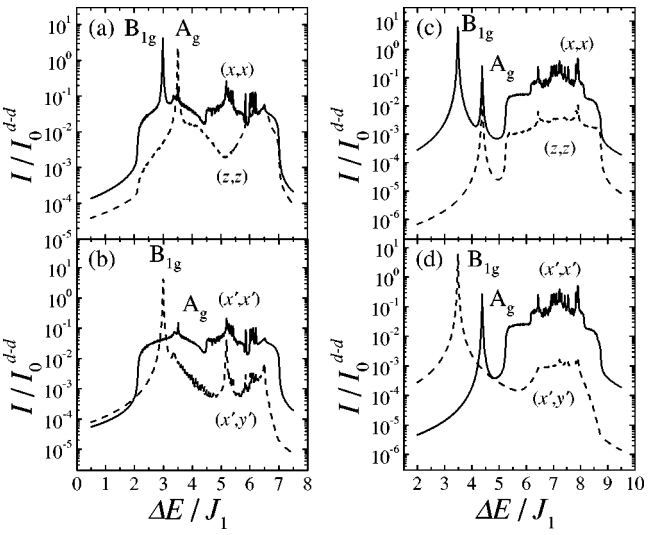

FIG. 4. Raman scattering spectra from the orbital waves in the d-d process. (a),(b) paramagnetic phase and (c),(d) A-AF phase. Parameter value is chosen to be $\tilde{J}_2/\tilde{J}_1=0.35$. Other parameter values are the same as those in Fig. 2.

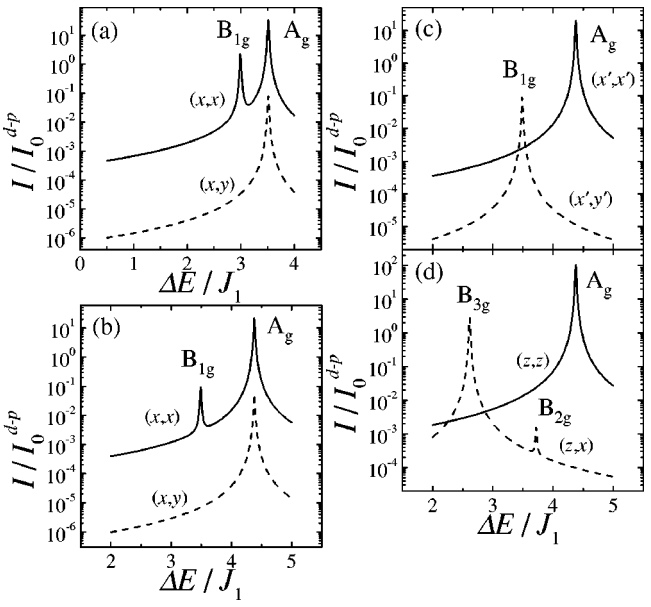

FIG. 5. Raman scattering spectra from the orbital waves in the d-p process. (a) The paramagnetic phase and (b)–(d) A-AF phase. The displacement of the O ions and the rotation of MnO_6 octahedra are chosen to be $\delta_1/l_{pd}=0.04$ and $\beta=\pi/18$. Other parameter values are the same as those in Fig. 2.

are prohibited. We notice the following relations of the relative intensity in the two-orbiton Raman spectra: $I(x,x) \sim I(x',x') > I(z,z) \gg I(x',y')$. These relations reflect the C-type orbital ordering with $\theta_{A1}^t=0.507\pi(0.481\pi)$ in the paramagnetic (A-AF) phase. In these orbital orderings, SE interaction between NN e_g electrons in the xy plane is much stronger than that along the z axis. Therefore, the intensity in the (z,z) polarization is smaller than those in the (x,x) and (x',x') polarizations. Small intensity in the (x',y') configuration is attributed to the interference effect between the orbitons with the different symmetry. In the spectra from two-orbiton excitations, several peaks and edges are shown. As the two-magnon Raman spectra reflect the density of states (DOS) of the magnon, the two-orbiton Raman spectra reflect the DOS of the orbiton. Position of the each peak corresponds to the van Hove singularity of the DOS of the orbiton.

B. d-p process

In Figures 5, numerical results of the Raman spectra in the d-p process are shown. Figures 5(a) and 5(b)–5(d) are the results in the paramagnetic and A-AF phases, respectively. I_0^{d-p} is defined as $I_0^{d-p}=\omega_f^2 C^2 N/[\hbar(2\pi)^2]\tilde{J}^2$ and is assumed to be independent of $\omega_{i,f}$, for simplicity. Parameter values are chosen to be $\delta_1/l_{pd}=0.04$ and $\beta=\pi/18$. Changes in the distance and transfer intensity between Mn and O ions are taken into account as a prefactor of ρ_ν in Eq. (26) up to the order of $O(\delta_1/l_{pd})$. Other parameter values are the same as those in Fig. 2. We find that the relative intensity of the two spectra from the A_g and B_{1g} modes in the (x,x) configuration in the d-p process is different from that in the d-d process, i.e., in the d-p process, the spectrum of the A_g mode becomes larger than that of the B_{1g} mode. As shown in Eq. (5), in the A_g mode, the orbital excitation at each site occurs in-phase. Therefore, the interference effect in the in-phase A_g mode increases its intensity in the d-p process. On the other hand, in the d-d process, orbital excitation is dominated by the process where the two electrons in the NN Mn sites are exchanged with each other. This reflects the AF-type orbital ordering in the ground state. A minus sign in the scattering matrix arises from the exchange of electrons and the interference effects are reduced.

C. Effect of the lattice distortion

It has been reported that the lattice structure of $LaMnO_3$ is of the monoclinic when the oxygen partial pressure during the synthesis is low.[39] A sample used in the recent Raman scattering experiments shows the monoclinic structure.[40] We examine the effect of the monoclinic distortion on the Raman spectra for the detailed comparison between the theory and the experiments.

We adopt a model of the monoclinic structure shown in Fig. 6. Displacements of the O ions indicated by arrows are considered up to the order of $O(\delta_i/l_{pd})$. The transfer intensity between NN Mn e_g orbitals in the xy plane is given by $t_0^{xy}(\delta)=t_0(0)(1+\delta/l_{pd})^{-3.5}(1-\delta/l_{pd})^{-3.5}$ and does not change in the order of $O(\delta_i/l_{pd})$. $J_{1,2}^{xy}[\propto(t_0^{xy})^2]$ does not change, either. On the contrary, t_{pd} changes as $t_{pd}(\delta)=t_{pd}(0)(1\pm 3.5\delta/l_{pd})$. This indicates the Raman spectra in the d-p process are sensitive to the the oxygen displacement. We concentrate on the d-p process, below.

In Fig. 7, the numerical results with the monoclinic distortion are shown. Here, the dispersion relation of the OW is calculated in the unit cell which includes eight Mn sites with the A-AF ordering. Parameter values are chosen to be $(\delta_1,\delta_2,\delta_3,\delta_4)/l_{pd}=(0.03,0.11,0.07,0.15)$, $\beta=\pi/18$ and $R=1.15$. Other parameters are the same as those in Fig. 2. We

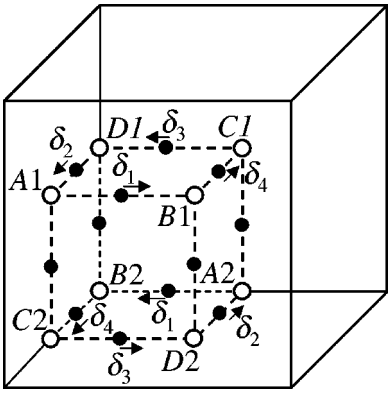

FIG. 6. A unit cell of the monoclinic structure (straight lines). Open and filled circles represent Mn and O ions, respectively. Broken lines show a unit cell of the cubic perovskite structure. The arrows indicate the displacement of O ions in the monoclinic structure where δ_i is the amplitude of the oxygen displacement. Alternate rotations of MnO_6 octahedra around x' axis are shown in Fig. 1(b).

show new spectra marked by *M*. Intensities of the new spectra are small compared with others reflecting the small monoclinic distortion. The new peaks at 3.6 J_1 and 4.4 J_1 originate from the breaking of the mirror symmetry perpendicular to the *z* axis in the monoclinic structure $P2_1/c$.[39] There also appear new peaks at 3.1 J_1. The peak position corresponds to the energy of the OW at the *X* point marked by an asterisk in Fig. 2(b). This mode becomes zone center mode and Raman active in the monoclinic structure.

Now, let us compare our theoretical results with the recent experimental ones reported in a single crystal of $LaMnO_3$.[28] In addition to the phonon Raman spectra below 100 meV,[32,33] the sharp spectra are observed at 120–170 meV(see the insets of Fig. 7). The OW is considered as an origin of the new spectra. In the Raman scattering experiment, the 514.5 nm (2.4 eV) line of an Ar^+ laser was used. The energy of the incident photon is expected to be almost the same as the electron excitation energy from O $2p$ to Mn e_g.[41] In this case, I_0^{d-p} is strongly enhanced compared with I_0^{d-d}.[42] Thus, the experimental results are compared with our theoretical ones with the monoclinic distortion in the *d-p* process. As shown in Fig. 7, the characteristic features of polarization dependence and relative intensity of the experimental Raman spectra in the region of 120–170 meV are well reproduced by our theoretical ones. Thus, the Raman spectra observed in the region of 120–170 meV in $LaMnO_3$ are attributed to the OW excitations.

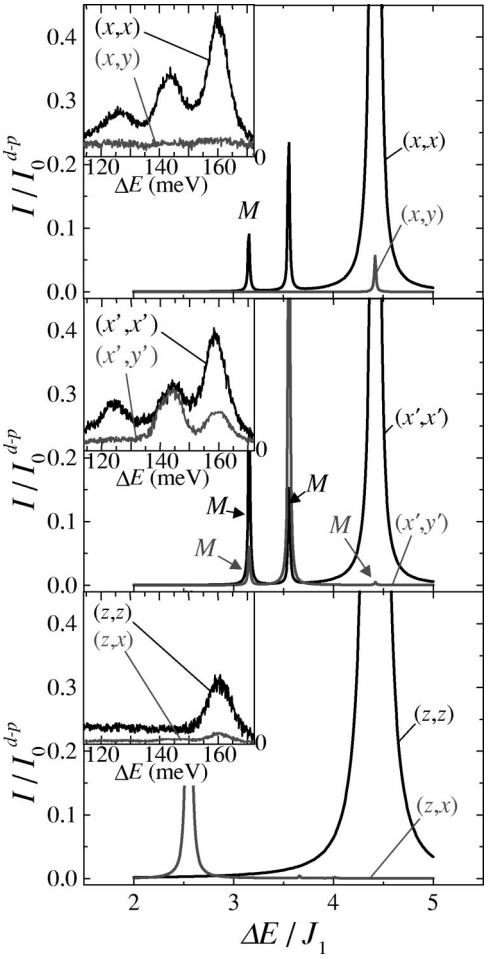

FIG. 7. Raman scattering spectra from the OW in the *d-p* process. The *A*-AF ordering and the monoclinic lattice distortion is assumed. The displacement of the O ions and the rotation of MnO_6 octahedra are chosen to be $(\delta_1,\delta_2,\delta_3,\delta_4)/l_{pd}=(0.03,0.11,0.07,0.15)$ and $\beta=\pi/18$. The anisotropy in the transfer intensity is chosen to be $R=1.15$. Other parameter values are the same as those in Fig. 2. Orbital state is given by $(\theta_{A1(2)},\theta_{B1(2)},\theta_{C1(2)},\theta_{D1(2)})=(\theta_A,-\theta_A,\theta_A,-\theta_A)$ with $\theta_A=0.47\pi$. Insets show the experimental Raman spectra in $LaMnO_3$ at 9 K in Ref. 28. Vertical axes of the experimental data are arbitrary.

VI. SUMMARY AND DISCUSSION

In this study, we have theoretically investigated the Raman scattering as a probe to detect the OW excitation in manganites. We proposed two excitation processes for the Raman scattering, i.e., the *d-d* and *d-p* processes. The *d-d* process is analogous to the two-magnon Raman scattering process in antiferromagnets. However, scattering intensity from one- and two-orbiton excitations are of the same order of magnitude. In the *d-p* process, photon induces transfer of electrons between Mn e_g and O $2p$ orbitals, and one-orbiton excitations are brought about. Because $LaMnO_3$ is a charge-transfer type insulator where the optical gap is about 1 eV, the *d-p* process is expected to dominate the Raman scattering using the visible light. It was shown that the theoretical results of the Raman spectra from the one-orbiton excitations well explain the experimental Raman spectra observed in $LaMnO_3$.

As mentioned in Sec. II, the OW in the *A*-AF phase has a gap originating from the anisotropic spin structure. We expect that the gap is suppressed by applying a magnetic field. This change will be detected as a shift of the peak positions of the spectra. The gap-less OW may also be observed in the ferromagnetic-insulating manganites such as $La_{0.88}Sr_{0.12}MnO_3$, where the orbital ordering is experimentally confirmed.[43] In Sec. V, we compared the theoretical

results in the d-p process with the experiments[28] by considering the incident photon energy. It is expected that the spectral intensities in the d-d process are enhanced with increasing the incident photon energy and resonating with the electron excitation between the lower and the upper Hubbard bands. When the Raman scattering experiment using such a high-energy photon is carried out in $LaMnO_3$, the Raman spectra from the two-orbiton excitations will be observed around 200–350 meV and much information of the OW will be obtained.

ACKNOWLEDGMENTS

The authors would like to thank Y. Tokura, E. Saitoh, T. Takahashi, K. Tobe, K. Yamamoto and T. Kimura for their valuable discussions and providing us experimental data before publication. Fruitful discussions with P. Prelovšek, G. Khaliullin, and K. Tsuda are also acknowledged. This work was supported by Grant-in-Aid for Scientific Research Priority Area from the Ministry of Education, Science, Sports, Culture and Technology of Japan, CREST Japan and Science and Technology Special Coordination Fund for Promoting Science and Technology. Part of the numerical calculation was performed in the supercomputing facilities in IMR, Tohoku University. One of the authors (S.M.) acknowledges support of the Humboldt Foundation.

APPENDIX: SYMMETRY PROPERTY OF ORBITAL WAVE

We present in this appendix the symmetry properties of OW introduced in Sec. II and their selection rules in the Raman scattering. It is shown that the irreducible representations of the modes $(-+)$, $(--)$, $(++)$, and $(+-)$ at $\vec{k}=0$ are identified as A_g, B_{2g}, B_{1g}, and B_{3g} in the D_{2h} group, respectively. From the irreducible representations, the allowed-mode symmetries of the orbital waves in several polarization configurations are assigned. In this paper, polarization configuration of incident and scattered photons is denoted by (ζ,η) with $\zeta,\eta=x,y,z,x',y'$. Here, x, y, and z axes are taken to be the directions of the bonds connecting NN Mn sites and $x'=x+y(y'=-x+y)$. x', z and $-y'$ axes correspond to a, b, and c axes in $Pnma$ structure, respectively (see Fig. 1). Polarization configurations and the allowed-mode symmetries of the orbital waves are summarized as follows:

$$(x,x)\rightarrow A_g+B_{1g},$$

$$(y,y)\rightarrow A_g+B_{1g},$$

$$(z,z)\rightarrow A_g,$$

$$(x,y)\rightarrow A_g,$$

$$(z,x)\rightarrow B_{2g}+B_{3g},$$

$$(x',x')\rightarrow A_g,$$

$$(x',y')\rightarrow B_{1g}.$$

*Present address: Department of Physics, Tohoku University, Sendai 980-8578, Japan.

[1] K. Chahara, T. Ohono, M. Kasai, Y. Kanke, and Y. Kozono, Appl. Phys. Lett. **62**, 780 (1993).
[2] R. von Helmolt, J. Wecker, B. Holzapfel, L. Schultz, and K. Samwer, Phys. Rev. Lett. **71**, 2331 (1993).
[3] Y. Tokura, A. Urushibara, Y. Moritomo, T. Arima, A. Asamitsu, G. Kido, and N. Furukawa, J. Phys. Soc. Jpn. **63**, 3931 (1994).
[4] Y. Tokura and N. Nagaosa, Science **288**, 462 (2000).
[5] J. B. Goodenough, Phys. Rev. **100**, 564 (1955); in *Progress in Solid State Chemistry*, edited by H. Reiss (Pergamon, London, 1971), Vol. 5.
[6] J. Kanamori, J. Phys. Chem. Solids **10**, 87 (1959).
[7] G. Matsumoto, J. Phys. Soc. Jpn. **29**, 606 (1970).
[8] K. Hirota, N. Kaneko, A. Nishizawa, and Y. Endoh, J. Phys. Soc. Jpn. **65**, 3736 (1996); F. Moussa, M. Hennion, J. Rodriguez-Carvajal, H. Moudden, L. Pinsard, and A. Revcolevschi, Phys. Rev. B **54**, 15 149 (1996).
[9] W. E. Pickett and D. J. Singh, Phys. Rev. B **53**, 1146 (1996).
[10] S. Satpathy, Z. S. Popović, and F. R. Vukajlović, Phys. Rev. Lett. **76**, 960 (1996).
[11] I. Solovyev, N. Hamada, and K. Terakura, Phys. Rev. Lett. **76**, 4825 (1996).
[12] S. Ishihara, J. Inoue, and S. Maekawa, Physica C **263**, 130 (1996); Phys. Rev. B **55**, 8280 (1997).
[13] Y. Murakami, J. P. Hill, D. Gibbs, M. Blume, I. Koyama, M. Tanaka, H. Kawata, T. Arima, Y. Tokura, K. Hirota, and Y. Endoh, Phys. Rev. Lett. **81**, 582 (1998).
[14] J. Rodriguez-Carvajal, M. Hennion, F. Moussa, A. H. Moudden, L. Pinsard, and A. Revcolevschi, Phys. Rev. B **57**, R3189 (1998).
[15] R. Maezono, S. Ishihara, and N. Nagaosa, Phys. Rev. B **57**, R13 993 (1998).
[16] L. F. Feiner and A. M. Oleś, Phys. Rev. B **59**, 3295 (1999).
[17] S. Okamoto, S. Ishihara, and S. Maekawa, Phys. Rev. B **65**, 144403 (2002).
[18] M. Cyrot and C. Lyon-Caen, J. Phys. (Paris) **36**, 253 (1975).
[19] G. Khaliullin and V. Oudovenko, Phys. Rev. B **56**, R14243 (1997).
[20] L. F. Feiner, A. M. Oleś, and J. Zaanen, J. Phys.: Condens. Matter **10**, L555 (1998).
[21] G. Khaliullin and R. Kilian, J. Phys.: Condens. Matter **11**, 9757 (1999).
[22] J. van den Brink, W. Stekelenburg, D. I. Khomskii, G. A. Sawatzky, and K. I. Kugel, Phys. Rev. B **58**, 10 276 (1998).
[23] V. Perebeinos and P. B. Allen, Phys. Status Solidi B **215**, 607 (1999).
[24] S. Ishihara, M. Yamanaka, and N. Nagaosa, Phys. Rev. B **56**, 686 (1997).
[25] S. Ishihara and S. Maekawa, Phys. Rev. B **62**, 2338 (2000).
[26] J. Inoue, S. Okamoto, S. Ishihara, W. Koshibae, Y. Kawamura, and S. Maekawa, Physica B **237-238**, 51 (1997).

[27] T. Inami, S. Ishihara, H. Kondo, J. Mizuki, T. Fukuda, S. Maekawa, H. Nakao, T. Matsumura, K. Hirota, Y. Murakami, and Y. Endoh, cond-mat/0109509 (unpublished).

[28] E. Saitoh, S. Okamoto, K. Takahashi, K. Tobe, K. Yamamoto, T. Kimura, S. Ishihara, S. Maekawa, and Y. Tokura, Nature (London) **410**, 180 (2001).

[29] T. Saitoh, A. E. Bocquet, T. Mizokawa, H. Namatame, A. Fujimori, M. Abbate, Y. Takeda, and M. Takano, Phys. Rev. B **51**, 13 942 (1995).

[30] J_1 and J_2 are defined as $J_1=t_0^2/(U'-I)$ and $J_2=t_0^2/(U'+I+2J_H)$, respectively, where a relation $U=U'+I$ is assumed. t_0 is the transfer intensity between NN $d_{3z^2-r^2}$ orbitals along the z axis. Energy splitting due to the JT effect is neglected in the denominators because the splitting is much smaller than the Coulomb interactions (Ref. 29).

[31] Pseudospin operator $\vec{T}_i$ is defined as $\vec{T}_i=(1/2)\Sigma_{\gamma\gamma'\sigma}\tilde{d}^{\dagger}_{i\gamma\sigma}(\vec{\sigma})_{\gamma\gamma'}\tilde{d}_{i\gamma'\sigma}$ where $\tilde{d}_{i\gamma\sigma}$ is the annihilation operator of the e_g electron at site i with spin σ and orbital γ without double occupancy.

[32] K. Yamamoto, Master thesis, University of Tokyo, 1996.

[33] M. N. Iliev, M. V. Abrashev, H.-G. Lee, V. N. Popov, Y. Y. Sun, C. Thomsen, R. L. Meng, and C. W. Chu, Phys. Rev. B **57**, 2872 (1998).

[34] S. Okamoto, S. Ishihara, and S. Maekawa, Phys. Rev. B **61**, 451 (2000); **61**, 14 647 (2000).

[35] P. A. Fleury and R. Loudon, Phys. Rev. **166**, 514 (1968).

[36] R. J. Elliott, M. F. Thorpe, G. F. Imbusch, R. Loudon, and J. B. Parkinson, Phys. Rev. Lett. **21**, 147 (1968).

[37] B. S. Shastry and B. I. Shraiman, Phys. Rev. Lett. **65**, 1068 (1990).

[38] J. C. Slater and G. F. Koster, Phys. Rev. **94**, 1498 (1954); W. A. Harrison, *Electronic Structure and the Properties of Solids, The Physics of the Chemical Bond* (Freeman, San Francisco, 1980).

[39] J. F. Mitchell, D. N. Argyriou, C. D. Potter, D. G. Hinks, J. D. Jorgensen, and S. D. Bader, Phys. Rev. B **54**, 6172 (1996).

[40] K. Tsuda, Y. Ogata, M. Tanaka, E. Saitoh, T. Kimura, and Y. Tokura (unpublished); Abstracts of the Meeting of the Physical Society of Japan (56th Annual Meeting, Tokyo, 2001) Part 3, p. 454.

[41] T. Arima, Y. Tokura, and J. B. Torrance, Phys. Rev. B **48**, 17 006 (1993); T. Arima and Y. Tokura, J. Phys. Soc. Jpn. **64**, 2488 (1995).

[42] The relative strength of the scattering intensity between the *d-d* and the *d-p* processes is estimated as follows. Using $l_{dd}\approx 2l_{dp}$ and $t_0\approx t_{pd}^2/\Delta$ with $t_{pd}\sim 1.8$ and $\Delta\sim 4.5$ eV (Ref. 29), and keeping the leading terms in I_0^{d-d} and I_0^{d-p}, we obtain $I_0^{d-d}/I_0^{d-p}\approx 0.4^2[(U'-I-\frac{3}{4}J_H-\Delta-\hbar\omega_{\vec{k}_i})/(U'-I-\hbar\omega_{\vec{k}_i})]^2$. The fraction of I_0^{d-d} is less than 20% when $\hbar\omega_{\vec{k}_i}<U'-I-(3/4)J_H-\Delta$.

[43] Y. Endoh, K. Hirota, S. Ishihara, S. Okamoto, Y. Murakami, A. Nishizawa, T. Fukuda, H. Kimura, H. Nojiri, K. Kaneko, and S. Maekawa, Phys. Rev. Lett. **82**, 4328 (1999).